Processing and electromechanical properties of lanthanum-doped Pb(Zr,Ti)O₃ extruded piezoelectric fibres

**F. Clemens · T. Comyn · J. Heiber ·
F. Nobre · A. C. E. Dent · C. R. Bowen**

Abstract This article describes the processing and characterisation of lanthanum-doped lead zirconate titanate (PLZT)-based ferroelectric fibres for composite transducer applications. X-ray diffraction of the extruded and sintered fibres indicated some lead loss during sintering; however, the fibres exhibited low porosity (1.54%), high maximum piezoelectric strain (4041 ppm) and relatively low coercive field (0.77 kV/mm). The low coercive field of the lanthanum-doped fibres may be advantageous in terms of facilitating polarization of the fibres in composite architectures.

Introduction

Composites containing highly aligned lead zirconate titanate (PZT) rods or fibres have been widely studied and utilized in sensor and actuator applications [1]. The recent commercial availability of fine-scale PZT fibres (<300 μm in diameter) of semi-continuous lengths has stimulated progress of both established and novel applications. Fine-scale PZT fibres were initially developed for use in medical ultrasound transducers, due to the improved imaging resolution provided by a reduction in the active element, or

fibre, size [2]. Piezoelectric fibres have also been considered for flexible ultrasonic transducers [3, 4]. The inclusion of active fibres in structural composites has also enabled the production of intelligent components capable of passive vibration control and damping [5] or even structural morphing [6]. Interest in piezoelectric fibres has also stemmed from developments in Active Fibre Composites (AFCs) which is a device that achieves actuation through the use of interdigitated electrodes (IDE) that apply a non-linear electric field in the plane of the composite and fibre direction [7]. The device consists of aligned fine-scale piezoelectric fibres embedded in a polymer matrix with IDEs on the upper and lower faces to apply an electric field along the fibre length, thus utilising the relatively high d_{33} piezoelectric strain coefficient. Significant advancements have been made in the materials, design, modelling and manufacture of AFC type devices, which has proven to be a fertile area of research [8]. The AFC configuration promises to offer advances in the field of active components and may prove pivotal for the realisation of intelligent structures.

A range of processing routes are currently used for commercial production of PZT fibres, including extrusion [9], viscous polymer processing (VPP) [10], viscose suspension spinning (VSSP) [11], Alceru spinning [12] and sol–gel processing [13]. Other processing methods have been investigated, such as relic processing [14] and PZT-coated inactive fibres [15]. The aim of this article is to explore for manufacture of lanthanum-doped Pb(Zr,Ti)O₃ piezoelectric fibres by extrusion in an attempt to manufacture high strain fibres for actuator or sensor applications. La-doping of PZT has been undertaken since it has the potential to provide a variety of benefits including increased squareness of the hysteresis loop, decreased coercive field, increased dielectric constant, high coupling coefficients and

F. Clemens (✉) · J. Heiber · F. Nobre
Laboratory for High Performance Ceramics, Empa, Swiss Federal Laboratories for Materials Science and Technology, Ueberlandstrasse 129, 8600 Duebendorf, Switzerland
e-mail: Frank.Clemens@empa.ch

T. Comyn
Institute for Materials Research, University of Leeds, Leeds LS2 9JT, UK

A. C. E. Dent · C. R. Bowen
Department of Mechanical Engineering, Materials Research Centre, University of Bath, Bath BA2 7AY, UK

increased mechanical compliance [16–18]. PLZT fibre syntheses have also been investigated for optoelectronic and ultrasonic imaging applications [19–22]. Mainly chemical phase and microstructure were investigated by the authors. None of these fibres have been investigated in terms of longitudinal free strain evolution (butterfly curve) hysteresis loop or optoelectronic properties. In this article, lanthanum doping is of particular interest in order to achieve a low coercive field (E_c). A low E_c will ease the polarization of the fibre along its axis via the complex electric field formed by the interdigitated electrodes.

Experimental

Powder fabrication

The initial powders used for the fibres were prepared using conventional mixed oxide synthesis. The constituent oxides (PbO, La_2O_3, ZrO_2 and TiO_2, Sigma–Aldrich) were dried, weighed in the correct proportions and milled for 1 h in 2-propanol, followed by drying and sieving. A high energy bead mill (Dynomill, Willy A. Bachofen) was used to produce a fine particle size. Care was taken during drying to prevent preferential sedimentation of the powders. Powders were calcined for 900 °C for 4 h in covered alumina crucibles, then milled, dried and sieved in the same manner. For the sieved powder, density was evaluated using a helium pycnometer (AccuPyc 1330, Micromeritics, USA) and the specific surface area was determined from a five point N_2 adsorption isotherm obtained from BET measurements (Beckman-Coulter SA3100, Beckman-Coulter, USA). The particle size distribution of the powders was measured with a laser diffraction analyzer (LS230, Beckman-Coulter, USA).

The intended target composition of the powders was $Pb_{0.94}La_{0.06}Zr_{0.58}Ti_{0.42}O_{3+\delta}$; the composition was PbO rich to compensate for potential lead loss during calcination and sintering. In the advent of lead loss, assuming there are negligible oxygen vacancies, the intended formula would be $Pb_{0.905}La_{0.06}Zr_{0.58}Ti_{0.42}O_3$.

Fibre fabrication

To manufacture fibres, a powder–polymer mixture (feedstock) with 58 vol.% of the PLZT powder was prepared in a high-shear mixer (Rheomix 600, Thermo Electron). The polymer binder was low density polyethylene (PEBD 1700 MN 18C, Lacqtene, Elf Atochem S.A.). Prior to compounding, the PLZT powder was pre-coated with stearic acid (Fluka, Sigma–Aldrich). The feedstock was then extruded through a ceramic die with a 300-μm-diameter orifice at 140 °C using a ram extruder. After extrusion, the fibres were sintered in a PbO-rich atmosphere at 1200 °C for 2 h.

Fibre characterisation

X-ray diffraction and crystallographic analysis

X-ray diffraction (XRD) was undertaken using Cu-Kα radiation (PANalytical X'Pert Pro Multipurpose Diffractometer, Netherlands). Wide-angle scans of 2θ were taken from 5° to 80° (Bragg–Brentano configuration) with a step width of 0.02 and an exposure time of 2 s per step (Cu-Kα radiation, 40 mA heating current, 40 kV beam potential). Rietveld analysis was performed on diffraction data (X'Pert HighScore Plus, PANalytical, Philips, Netherlands) to determine the phase, lattice parameters and fractional coordinates.

Shrinkage, porosity and grain size

Sintering shrinkage was measured from the mean fibre diameter in the 'green' state and after sintering [23]. For the microstructure analysis, a fibre was longitudinally embedded into cold resin (Technorit 4000, Heraeus Kulzer GmbH, D), ground and polished as described by Heiber et al. [23]. Scanning electron microscopy (SEM; Vega Plus 5136MM, Tescan) on polished samples (ten images) was used to assess the porosity using image analysis (Digital Micrograph 3.10.0, Gatan). Grain size was measured after chemical etching by the linear intercept method using three images at different areas of the fibre cross section [24]. Visual examination was undertaken to observe any colour changes due to lead oxide loss or adherence of fibres during sintering.

Microscopy and energy dispersive X-ray (EDX)

Electron micrographs were obtained for fibre cross sections, employing EDX analysis to assess compositional fluctuations across the fibre using a Leo Gemini 1530 FEG-SEM, Cambridge, UK and EDX (Inca, Oxford Instruments, UK). The degree of volatile PbO loss whilst sintering the fibres was examined. Samples were mounted in epoxy, and progressively diamond polished with finer media to a final size of 1 μm. Samples were carbon coated prior analysis to alleviate the effects of charging.

Electromechanical measurements on fibres

The electromechanical properties were tested on single fibres by means of a single fibre test method [25]. For characterisation, 3.5-mm long fibres were fixed vertically inside a PMMA holder. At both end of the fibres, silver

epoxy (Electrodag 5915, Acheson Colloids Company) was used as contact electrodes. After sample preparation, the active free length of the fibres was thereby shortened to about 2.5 mm. To avoid electrical breakdown, the fibres were immersed in silicon oil. Sintered fibres were polarized by applying an electric field of 3.5 kV/mm for 5 min. The free strain (S) evolution for the single fibres as function of the applied electric field (E, ±3 kV/mm) was measured at a frequency of 2.778 mHz by using a Dynamic Mechanical Analyzer (Perkin–Elmer DMA 7e). The investigation was undertaken on five fibres.

Results

Powder properties

After the calcination stage, the powder properties were investigated to be able to calculate the appropriate composition of the feedstock for fibre extrusion, namely the amount of stearic acid and binder content. The results a shown in Table 1 and the particle size results indicates a fine and narrow distribution.

XRD and structure refinement

The perovskite structure was determined using a Rietveld analysis, for the fibre sintered at 1200 °C in a PbO atmosphere. For this analysis, tetragonal (P4mm) and rhombohedral (R3m), and a mixture were fitted for the intended final composition of $Pb_{0.91}La_{0.06}Zr_{0.58}Ti_{0.42}O_3$ using a provisional temperature factor of 1 Å^2 for all atoms and zero atomic displacements within the unit cell

(centrosymmetric). The starting point for the lattice parameters was calculated from the XRD peak at ca. 22°, in order to ensure convergence using a Rietveld refinement only very approximate initial values are required, for example the same value can be used for the a- and c-lattice parameters in the tetragonal phase (Table 2). Figure 1 shows the outcome of the structural refinement; an extremely good fit is achieved using a tetragonal model only, i.e. without the inclusion of rhombohedral phase. The lattice
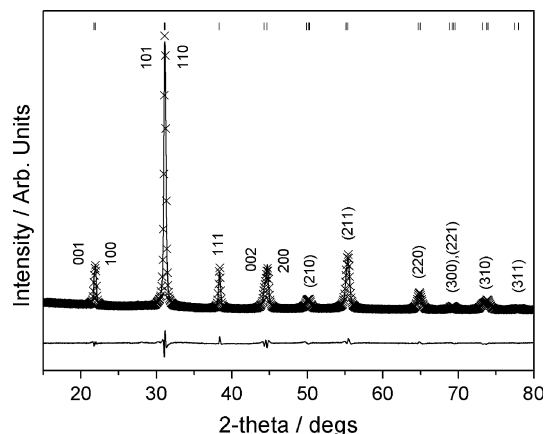

Fig. 1 Structural refinement for $Pb_{0.905}La_{0.06}Zr_{0.58}Ti_{0.42}O_3$ sintered at 1200 °C in a PbO atmosphere. $R_{exp} = 1.553$, $R_p = 3.589$, $R_{wp} = 4.494$. The raw data is shown with crosses (only one in four data points are shown to improve clarity), with the accompanying fit (*solid line*). The residuals from the refinement are shown by the *solid line* below. *Tickmarks* associated with the tetragonal phase are shown at the top

Table 1 Powder properties of powders used for fibre production

d_{10} (μm)	0.6
d_{50} (μm)	1.1
d_{90} (μm)	2.1
Density (g/cm^3)	7.85
BET (m^2/g)	2.181

Table 2 Initial parameters used for Rietveld refinement

	P4mm		R3m	
Temperature Factor, B/Å^2	1		1	
Lattice parameters/Å	a	c:	a:	c:
	4.06	4.06	5.74	14.06
Atomic coordinates				
A-site (Pb,La)	0,0,0		0,0,0	
Bi-site (Zr,Ti)	½,½,½		0,0,¼	
O$_1$	½,0,½		½,0,0	
O$_2$	½,½,0		–	

Table 3 Refined parameters for fibres sintered at 1200 °C, in a PbO atmosphere

Atom	Temperature factor/Å^2	Fractional atomic coordinate	Refined occupancy
Pb	1.566	0,0,0	0.875
La	1.566	0,0,0	0.06[a]
Zr	0.419	½,½,0.534	0.600
Ti	0.419	½,½,0.534	0.381
O$_1$	1.361	½,0,0.581	1[a]
O$_2$	1.361	½,½,0.081	1[a]

[a] Refinement of these parameters led to the generation of inaccurate values and/or divergence

Table 4 EDX results of manufactured fibres

Element	Concentration (at.%)
Pb	13.21
La	0.85
Zr	10.15
Ti	6.7
O	69.1

Table 5 Comparison of intended, XRD and EDX occupancies

Element	Intended occupancies ($Pb_{0.91}La_{0.06}Zr_{0.58}Ti_{0.42}O_3$)	XRD occupancies	EDX occupancies
Pb	0.91	0.875	0.822
La	0.06	0.06[a]	0.053
Zr	0.58	0.600	0.632
Ti	0.42	0.381	0.417
O_1	2	2[a]	2
O_2	1	1[a]	1

[a] Refinement of these parameters led to the generation of inaccurate values and/or divergence

parameters are $a = 4.059$ Å and $c = 4.092$ Å, providing a spontaneous strain of $(c - a)/a = 0.80\%$. Results from the structural refinement outcome are shown in Table 3. The concentration of tetragonal phase was 100%. The agreement indices from the refinement are goodness of fit = 8.41%, $R_P = 3.59\%$ and $R_{WP} = 4.5\%$.

Microscopy and EDX

Energy dispersive X-ray was undertaken to provide elemental maps and line profiles, including a high count average in the centre of the sample. The results in atomic%
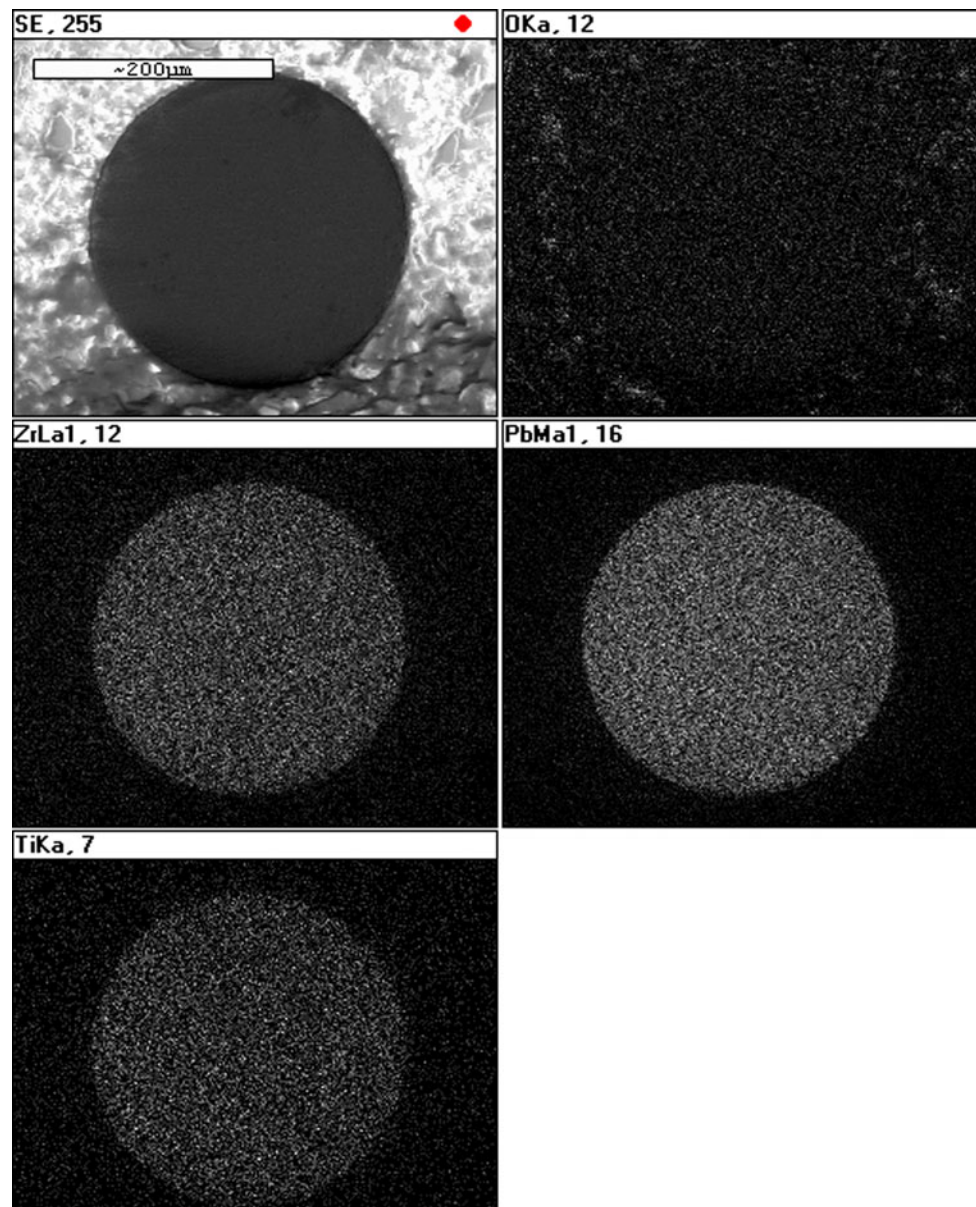

Fig. 2 Profile mapping using EDX; **a** secondary electron image, **b** O, **c** Zr, **d** Pb and **e** Ti elemental maps of fibre
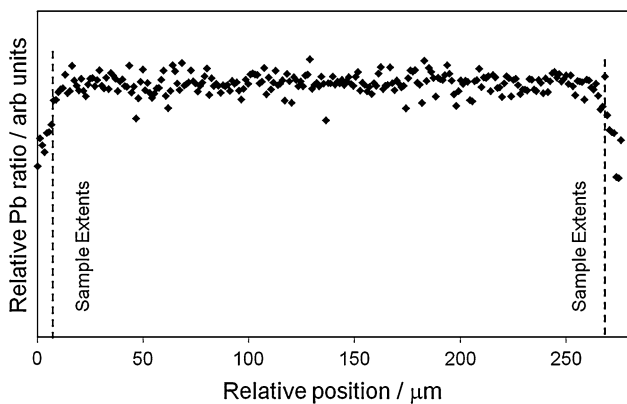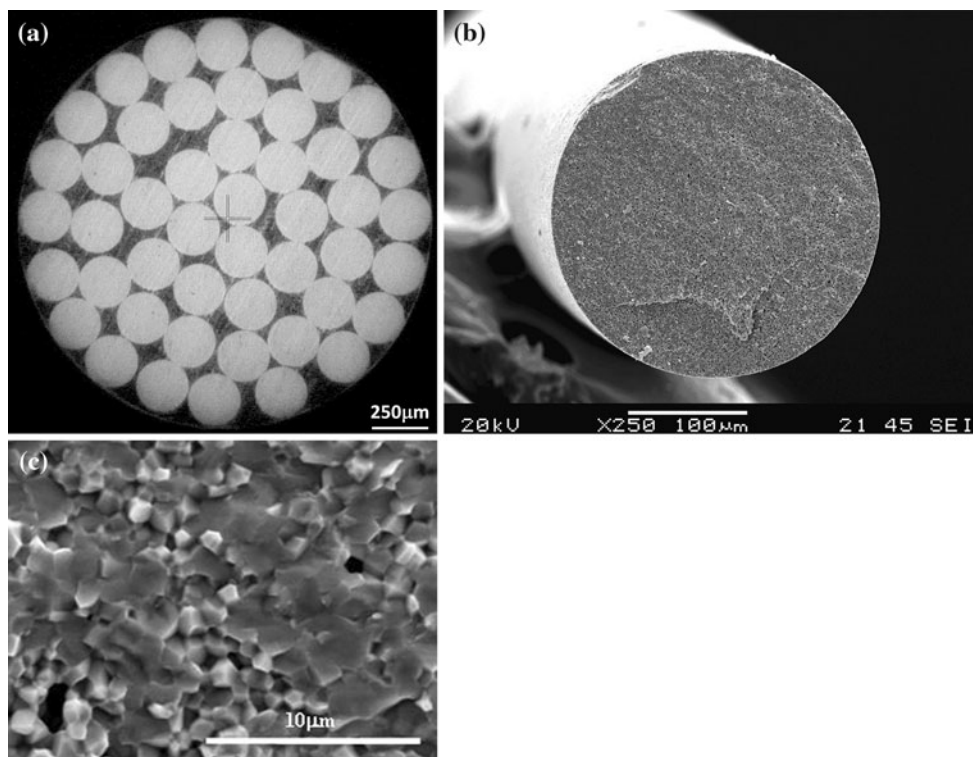
Fig. 3 Line maps across fibre section. Profile relates to a horizontal section across Fig. 2a

are shown in the Table 4. The oxygen concentration determined by EDX is unreliable, due to its low atomic number, and is therefore discounted. To assess the composition of the sintered fibres, and compare it with the intended composition $(Pb_{0.91}La_{0.06}Zr_{0.58}Ti_{0.42}O_3)$ and XRD results the total charge of the cations was set to 6 (as should be the case in a perovskite) and the occupancies determined. The intended and the measured formulae/composition from both EDX and XRD are shown in Table 5. Both of these techniques suggest, even with the utmost care, some lead loss has occurred in these materials

as a result of the calcination and sintering stages of fibre manufacture.

Profile mapping of the fibres, as shown in Fig. 2, suggest limited composition fluctuations as a function of location across the fibre diameter. It was not possible to extract accurate plots for the La concentration, due to the low relative proportions of this cation. A line profile across a sample is shown in Fig. 3, and relates to a line drawn horizontally across the first image in Fig. 2. In order to estimate the Pb concentration and loss, the ratio of the Pb count intensity was compared to the sum of the other elements. This was necessary as a variation in intensity was common to all elements at the edges compared to the centre, possibly due to topological effects such as rounding of the sample during polishing. As with the profile maps, the line profiles show a minor reduction in the relative Pb concentration as a function of position at the edges in the last ca. 10 μm; this may well be due in part to the effect of spot size and the relatively large interaction volume that is probed during EDX analysis. Figure 4a shows a number of fibres embedded in an epoxy in a 1–3 composite array to examine the cross section of a number of fibres. Figure 4b, c shows SEM images of a side-view and the final microstructure of a sintered fibre, respectively. The fibre cross section is consistent along the fibre and between fibres, which is of importance to avoid defects (such as air-gaps) between the electrode and active material layer in

Fig. 4 **a** 1–3 composite of manufactured fibres, **b** side-view and **c** microstructure of sintered fibre

composite devices which can reduce performance or accelerate device failure during poling at high electric fields [10].

Fibre characterisation

Table 6 provides details of the manufactured fibres sintered at 1200 °C for 2 h in a PbO atmosphere (e.g. shrinkage, porosity, grain size and electromechanical properties). The shrinkage was approximately 16% and no observable colour changes and low adherence of fibres post-sintering. A high sintered density was achieved with a low amount of open porosity, 1.54%. The grain size of 1.02 μm is relatively small compared to other fibres [26, p 544; 27]. Figure 5 shows a strain-field loop of the manufactured fibres and the maximum strain, saturation strain and coercive field measured from the strain-field loop are summarised in Table 5. The saturation strain is higher than Alceru, extruded, and VSSP fibres reported in [10, 26, p 544] and is equivalent to the high performance VPP fibres reported by Button et al. [10]. The 0.76-kV/mm coercive field of the fibres manufactured in this study is

lower than all of the fibres reported in [26, p 544], which are all above 1 kV/mm. The relatively low coercive field is possibly the result of lanthanum doping [18, 28]. While the manufacture of thin lanthanum-doped fibres have been reported in the literature [21, 29, 30], the coercive field has rarely been measured. The low coercive field of the fibres reported here can aid the polarization of composite materials, in particular when the presence of interdigitated electrodes produces a highly non-linear electric field distribution.

Conclusions

This article has examined the manufacture of lanthanum-doped $Pb(Zr,Ti)O_3$ fibres by extrusion. XRD, EDX and microscopy has been used to characterise the fibre compositions along with analysis of gain size, porosity and sintering shrinkage. A high sintered density was achieved in these materials with a low grain size (1.02 μm). The maximum and saturation strain were high compared to many other reported fibres and equivalent to high performance VPP fibres. More significantly, the fibres reported in this article exhibited a lower coercive field compared to may other available fibres. A low coercive filed can aid the polarization of composite structures with a complex electric field formed by interdigitated electrodes, making them potentially useful for active fibre composite applications. EDX and XRD indicate that some lead loss has occurred during processing and a high tetragonal content, indicating that potentially improved properties may be achieved by further control of processing conditions and PbO volatilization.

Table 6 Characterisation and condition data collected for extruded sintered fibres

Sintering shrinkage (%)	15.9 ± 0.93
Colour change	No
Adherence of fibres	Low
Porosity (%)	1.54 ± 0.67
Grain size (μm)	1.02 ± 0.14
Maximum strain (ppm)	4041 ± 54
Saturation strain, S_r (ppm)	1887 ± 20
Coercive field, E_c (kV/mm)	0.766 ± 0.048
S_r/maximum strain	0.47

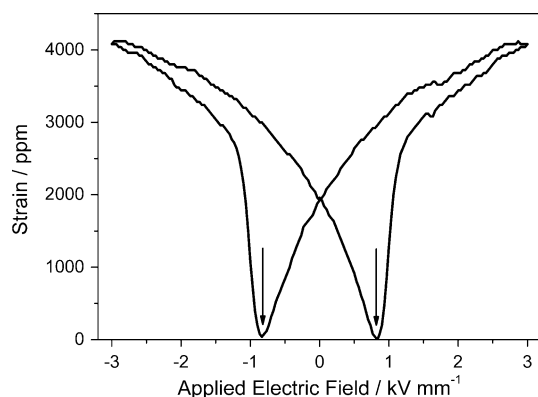Sintering temperature used was 1200 °C/2 h in a PbO atmosphere

Fig. 5 Strain–electric field loop of manufactured fibres. *Arrows* indicate coercive field

References

1. Tressler JF, Alkoy S, Doganand A, Newnham RE (1999) Composites A 30:477
2. Janas V, Safari A (1995) J Am Ceram Soc 78:2945
3. Harvey G, Gachagan A, Mackersie JW, Mccunnie T, Banks R (2009) IEEE Trans Ultrason Ferroelectr Freq Control 56:1999
4. Bowen CR, Bradley LR, Almond DP, Wilcox PD (2008) Ultrasonics 48:367
5. Yoshikawa S, Selvaraj U, Brooks KG, Kurtz SK (1992) In: Lui M (ed) Proceedings of the 8th IEEE International Symposium on applications of ferroelectrics, IEEE, New York, p 269
6. Schultz MR, Hyer MW, Williams RB, Wilkie WK, Inman DJ (2006) Compos Sci Technol 66:2442
7. Bent AA, Hagood NW (1997) J Intell Mater Syst Struct 8:903
8. Nelson LJ (2002) Mater Sci Tech 18:1245
9. Heiber J, Clemens F, Graule T, Hulsenberg D (2005) Adv Eng Mater 7:404
10. Bowen CR, Stevens R, Nelson LJ, Dent AC, Dolman G, Su B, Button TW, Cain MG, Stewart M (2006) Smart Mater Struct 15:295

11. Cass RB (1991) Am Ceram Soc Bull 70:424
12. Meister F, Vorbach D, Niemz F, Schulze T (2003) Materialwiss Werkstofftech 34(3):262
13. Li K, Li J, Cao D, Li J-H (2008) J Compos Mater 42:1125
14. Ting SM, Janas VF, Safari A (1996) J Am Ceram Soc 79:1689
15. Beckert W, Kreher W, Braue W, Antre M (2001) J Eur Ceram Soc 21:1445
16. Haertling GH, Land CE (1971) J Am Ceram Soc 54(1):1
17. Härdtl KH (1976) Ferroelectrics 12(1–4):9
18. Haertling GH (1999) J Am Ceram Soc 82:797
19. Meyer RJ, Shrout TR, Yoshikawa S (1997) In: ISAF '96—Proceedings of the 10th IEEE International Symposium on Applications of Ferroelectrics, vol 1 and 2. East Brunswick, p 547
20. Kitaoka K, Kozuka H, Yoko T (1998) J Am Ceram Soc 81(5):1189
21. Chong SL, Venkatesh R, Ramanan SR (2005) Integr Ferroelectr 70:19
22. Yu G, Wang X, Zhu L, Xu D, Ren Q, Zhang G, Liu X, Sun Z, Fan H (2008) Solid State Sci 10:859
23. Heiber J, Clemens F, Helbig U, De Meuron A, Soltmann CH, Graule T, Hulsenberg D (2007) Acta Mater 55:6499
24. Chinn RE (2002) In: Preparation and analysis of ceramic microstructures. ASM International, Materials Park
25. Belloli A, Heiber J, Clemems F, Ermanni P (2009) J Intell Mater Syst Struct 20:355
26. Nelson LJ, Bowen CR, Stevens R, Cain M, Stewart M (2003) In: Proceedings of the Society of Photo-optical Instrumentation Engineers (SPIE), vol 5053. Bellingham, p 544
27. Dent AC, Nelson LJ, Bowen CR, Stevens R, Cain M, Stewart M (2005) J Eur Ceram Soc 25:2387
28. Jiang QY, Subbarao EC, Cross LE (1994) J Appl Phys 75:7433
29. Li K, Li JH, Li JC, Chan HLW (2004) J Inorg Mater 19:361
30. Zhu ZL, Tang DY, Zhang XH, Qiao YJ (2010) Adv Mater Res 105–106:355